Journal of Materials Chemistry B

ROYAL SOCIETY OF CHEMISTRY

PAPER

View Article Online
View Journal | View Issue

Cite this: *J. Mater. Chem. B*, 2024, **12**, 10949

Mercaptoimidazole-capped gold nanoparticles as a potent agent against plant pathogenic fungi†

Tang Xu,‡[abd] Wenshuai Hao,‡[cg] Ran Du,‡[b] Dai Dai,[e] Cuixia Wang,[a] Suhua Li,[b] Carol Sze Ki Lin,[f] Ruitao Cha,*[ch] Jianbin Yan*[b] and Chong Li*[a]

Received 13th May 2024,
Accepted 18th September 2024

DOI: 10.1039/d4tb01032a

rsc.li/materials-b

Plant pathogenic fungi pose a substantial challenge to agricultural production, but the conventional fungicide-based approaches are losing importance. As agents with broad-spectrum antibacterial effects, gold nanoparticles (Au NPs) are found to have antifungal effects; however, no study has examined their application in agriculture as fungicides. Accordingly, this study investigates the activity of 2-mercaptoimidazole-capped Au NPs (MI-Au NPs) against the 'top' plant pathogenic fungi, finding that they could inhibit *Magnaporthe oryzae*, *Botrytis cinerea*, *Fusarium pseudograminearum* and *Colletotrichum destructivum* by inducing cytoplasmic leakage. Moreover, MI-Au NPs are found to protect plants from infection by *B. cinerea*. Specifically, pot experiments demonstrate that MI-Au NPs decrease the incidence rate of *B. cinerea* infection in *Arabidopsis thaliana* from 74.6% to 6.2% and in *Solanum lycopersicum* from 100% to 10.9%, outperforming those achieved by imazalil. Furthermore, the biosafety assays reveal that MI-Au NPs cannot penetrate the cuticle of plant cells or negatively influence plant growth, and it is safe to mammalian cells. In summary, the findings of this study will support the development of NP-based antifungal agents for use in agriculture.

1 Introduction

Plant pathogenic fungi pose a substantial challenge to global agricultural production, causing an annual crop loss of 10–20% that is equal to US$100–$200 billion.[1] Plant pathogenic fungi that destroy the most crops are *Magnaporthe oryzae*, *Botrytis cinerea*, *Fusarium graminearum*, *Fusarium oxysporum*, *Colletotrichum* spp. and so forth.[2] In particular, *M. oryzae* is a devastating cereal pathogen that causes neck rot and panicle blast, which can cause up to 80% rice loss during severe outbreaks. *B. cinerea* primarily affects the horticultural crops, leading to annual losses of US$10–$100 billion.[3] Currently, broad-spectrum fungicides such as mancozeb and chlorothalonil are employed as control strategies to mitigate fungal damage to crops.[4,5] However, over the past 50 years, there has been a concerning increase in the number of plant pathogenic fungi that have developed resistance to fungicides.[6] For example, *B. cinerea* is considered to have a high risk of rapidly developing resistance to fungicides due to the mutations that modify the target gene of fungicides and overexpression of drug efflux transporters.[7] Resistance of *B. cinerea* to new fungicides, such as benzimidazole, dicarboximide, and diethofencarb, has been observed only a few years after their application.[8] This has led to the emergence of nanoparticles (NPs) as a promising alternative.

Studies have demonstrated that various types of NPs can impede bacterial growth by preventing or overcoming biofilm formation. Silver-based NPs (Ag NPs) and gold-based NPs (Au NPs) have displayed efficacy in this regard by disrupting bacterial cell membranes, generating reactive oxygen species, penetrating bacterial cell membranes, or inducing intracellular antibacterial effects.[9] Their diminutive sizes endow them with

[a] *Kunpeng Institute of Modern Agriculture at Foshan, Shenzhen Branch, Guangdong Laboratory of Lingnan Modern Agriculture, Agricultural Genomics Institute at Shenzhen, Chinese Academy of Agricultural Sciences, Shenzhen, China. E-mail: lichonglx@caas.cn*

[b] *Shenzhen Branch, Guangdong Laboratory for Lingnan Modern Agriculture, Shenzhen Key Laboratory of Agricultural Synthetic Biology, Genome Analysis Laboratory of the Ministry of Agriculture and Rural Affairs, Agricultural Genomics Institute at Shenzhen, Chinese Academy of Agricultural Sciences, Shenzhen, China. E-mail: jianbinlab@caas.cn*

[c] *Laboratory of Theoretical and Computational Nanoscience, CAS Center for Excellence in Nanoscience, National Center for Nanoscience and Technology, Beijing 100190, China. E-mail: chart@nanoctr.cn*

[d] *School of Life Sciences, Henan University, Kaifeng 475004, China*

[e] *Department of Environmental Systems Science, ETH Zürich, Zurich 8092, Switzerland*

[f] *School of Energy and Environment, City University of Hong Kong, Hong Kong, China*

[g] *Biomanufacturing Center, Department of Mechanical Engineering, Tsinghua University, Beijing 100084, China*

[h] *NMPA Key Laboratory for Quality Research and Evaluation of Pharmaceutical Excipients, National Institutes for Food and Drug Control, 2 Tiantan Xi Li, Beijing, 100050, China*

† Electronic supplementary information (ESI) available. See DOI: https://doi.org/10.1039/d4tb01032a

‡ These authors made equal contributions.

unique characteristics (*e.g.*, enhanced cellular interaction), and potential for versatile and controllable applications.[10] When combined with antibacterial agents such as organic compounds or antibiotics, they exhibit a synergistic effect against pathogenic bacteria.[11] Furthermore, Ag NPs have demonstrated activity against a diverse array of plant pathogens, such as *B. cinerea*, *F. oxysporum* and *Cladosporium cucumerinum*.[12] The antifungal efficacy of Ag NPs could be even maximized by reducing their size or increasing the concentration.[13] Nevertheless, akin to chemical pesticides, the repeated use of Ag NPs can result in microbial resistance.[14]

Au NPs have gained increasing interest due to their good biocompatibility and ability to effectively exert antimicrobial activity.[15,16] Au NPs can be coated with various ligands such as a non-ionic chemical polyethylene glycol, or conjugated with small molecules such as antibiotics. These modifications enhance Au NPs' stabilities and antimicrobial activities.[17] For instance, the combination of *N*-heterocyclic prodrugs (*e.g.*, chloroauric acid, $HAuCl_4$) with Au NPs can endow the NPs with optimal antibacterial activities.[18] 4-Amino-2-pyrimidinethiol-capped Au NPs, 2,4-diamino-6-pyrimidinethiol-capped Au NPs, and negatively charged 4,6-dihydroxyl-2-pyrimidinethiol-capped Au NPs could inhibit the growth of clinically isolated multidrug-resistant *Escherichia coli* and *Pseudomonas aeruginosa*.[19] Functional Au NPs are potent agents against multi-drug-resistant bacteria.[20] Studies reported that bacteria take a longer timeframe to develop resistance to Au NPs than to Ag NPs, indicating that resistance to the former involves more complicated mechanisms. Even if the resistance is acquired, the antibacterial activities of Au NPs can be effectively restored by tuning the sizes or functional groups on the surface.[16,20] Currently, Au NPs have been applied to combat pathogenic fungi in medical research, finding that they could significantly inhibit the growth of *Candida albicans*[21,22] and *Aspergillus* spp.,[21–23] *in vitro*. However, to the best of our knowledge, no study has ever examined the activity of Au NPs against plant pathogenic fungi or reported their applications in agriculture.

Following the previous studies,[18,19] the objectives of this study were to investigate whether the functionalized Au NPs, with effective antibacterial efficacy, were active against plant pathogenic fungi and to evaluate their applications in agriculture. First, the effects of 2-mercaptoimidazole (MI)-capped Au NPs (MI-Au NPs) and 4,6-diamino-2-pyrimidinethiol (DAPT)-capped Au NPs (D-Au NPs) on selected plant pathogenic fungi including *B. cinerea*, *M. oryzae*, *F. pseudograminearum*, *C. destructivum*, *F. oxysporum*, and *F. graminearum* were investigated in disk diffusion tests, with 'naked' Au NPs (N-Au NPs) and imazalil being used as the controls. Next, scanning electron microscopy (SEM), transmission electron microscopy (TEM), and laser scanning confocal microscopy (LSCM) were applied to explore the mechanisms of Au NPs' antifungal action. Subsequently, detached leaf and pot experiments were carried out to evaluate the ability of MI-Au NPs to protect plants from infection with *B. cinerea*. Finally, the biological safety of MI-Au NPs was evaluated by examining their effect on plant growth and development, and on human umbilical vein endothelial cells (HUVECs) (Fig. 1).

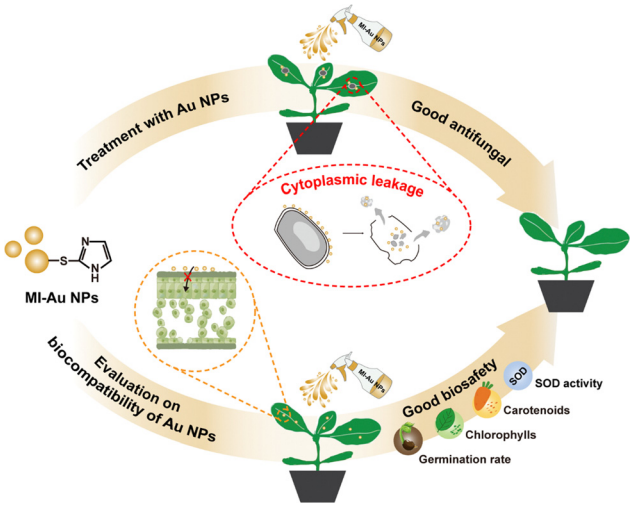

Fig. 1 Schematic diagram summarizing the protection effect of MI-Au NPs on plants against pathogenic fungi infection. MI-Au NPs could induce cytoplasmic leakage of *B. cinerea*, thereby inhibiting their growth and preventing their infection to plants in pot experiments. MI-Au NPs could not stunt plant growth or development, demonstrating its safety in use in agriculture.

2 Experimental

2.1 Materials

Chloroauric acid trihydrate ($HAuCl_4 \cdot 3H_2O$) and sodium borohydride ($NaBH_4$) were purchased from Merck (Shanghai, China). 4,6-Diamino-2-pyrimidinethiol (DAPT) and 2-mercaptoimidazole (MI) were purchased from Aladdin (Shanghai, China). Imazalil was purchased from Glpbio (USA). Oatmeal agar (OA) medium, potato dextrose agar (PDA) medium, and potato dextrose broth (PDB) medium were purchased from Coolaber (Beijing, China). Solid Murashige and Skoog (MS) medium was purchased from Sigma-Aldrich (USA). Propidium iodide (PI), disodium ethylenediaminetetraacetic acid (Na_2-EDTA), and nitroblue tetrazolium (NBT) were purchased from Coolaber (Beijing, China). Phosphate buffered saline (PBS), glutaraldehyde, osmium tetroxide (OsO_4), and fetal bovine serum (FBS) were purchased from Sigma-Aldrich (USA). Dulbecco's modified Eagle's medium (DMEM) was purchased from VivaCell (Shanghai, China). Penicillin–streptomycin solution was purchased from Biological Industries (Israel).

S. lycopersicum 'Ailsa Craig' (AC) seeds, *A. thaliana* (Columbia-0) seeds, and *B. cinerea* were kept at the Agricultural Genomics Institute, Chinese Academy of Agricultural Sciences (Shenzhen, China). *M. oryzae* was kindly provided by Dr Qun Liu of the China National Rice Research Institute (Hangzhou, China). *F. pseudograminearum*, *C. destructivum*, *F. oxysporum*, and *F. graminearum* were kindly provided by Dr Chengqi Zhang of Anhui Agricultural University (Hefei, China).

2.2 Preparation and characterization of NPs

MI-Au NPs, D-Au NPs, and N-Au NPs were prepared according to the literature.[18,19] Specifically, MI (0.1 mmol, dissolved in 10 mL of methanol, 200 μL of absolute acetic acid and 40 mg of Tween 80) and $HAuCl_4 \cdot 3H_2O$ (0.1 mmol, dissolved in 20 mL of

methanol) were mixed and stirred in an ice-water bath for 10 mins. $NaBH_4$ (0.3 mmol, dissolved in 5 mL of methanol) was then added dropwise with vigorous stirring. When the solution turned deep red, we decreased the stirring speed but kept stirring for another hour in the ice-water bath. Subsequently, we removed methanol in a vacuum at 40 °C, and an appropriate volume of deionized water was added to the residue. The solution was dialyzed (14 kDa molecular-weight cutoff, Millipore) for 48 h with deionized water, diluted with water and sterilized through a 0.22 μm filter (Millipore). The filtrate was stored at 4 °C until required. D-Au NPs and N-Au NPs were prepared in an analogous fashion; a 1 : 1 molar ratio of DAPT to $HAuCl_4 \cdot 3H_2O$ was used for the preparation of D-Au NPs, whereas N-Au NPs did not contain ligands.

The Au concentrations of all NPs were measured and determined by inductively coupled plasma-optical emission spectrometry (ICP-OES, Optima 5300DV, Perkin-Elmer, USA). First, the gold standard solution (1000 μg mL^{-1}, GSB 04-1715-2004, Guobiao Testing & Certification Co., Ltd, Beijing) was stepwise diluted to obtain solutions with selected concentrations (0.1, 1, 5, 10, and 25 μg mL^{-1}). The solution samples were then introduced to the plasma *via* a standard cross-flow nebulizer and Scott spray chamber (RF generator has a forward power of 1300 W with plasma, auxiliary and nebulizer gases set at 15, 0.5 and 0.8 L min^{-1}, respectively). A 0.1 s integration time with a fixed read time of 20 s and 5 points per peak provides consistent counting statistics (emission line at 242.80 nm). A standard curve describing the relationship between Au concentration and signal intensity was drawn with an R square greater than 0.996. Afterwards, Au NP samples were dissolved in freshly prepared aqua regia, diluted to 10 mL with ultrapure water and measured by ICP-OES under the same operation conditions. The concentrations of Au NPs were calculated according to the standard curve. The hydrodynamic sizes, size distributions, and zeta potentials of NPs were determined using a Zetasizer Nano ZS (Malvern, UK). The morphologies of NPs were obtained by TEM (HT-7700, Hitachi, Japan) according to the literature.[24] All measurements were performed three times.

2.3 Preparation of fungal spores and plants

Several of the reported top fungal pathogens in molecular plant pathology[2] were selected in this study. *M. oryzae* was cultivated on OA medium at 28 °C in darkness for 3 days, grown upright at 25 °C in light for 4 days, and then incubated at 28 °C in darkness for 10–12 days. *B. cinerea* was cultured on PDA medium at 23 °C in darkness for 10–12 days. *F. pseudograminearum*, *F. oxysporum*, and *F. graminearum* were cultured on PDA at 28 °C in darkness for 5–7 days, whereas *C. destructivum* was cultured on PDA at 28 °C in darkness for 12–14 days. All fungi were cultured statically until sufficient spores could be collected.

As one of the most commonly used model plants, *A. thaliana* (Columbia-0) was selected as a research object here. As one of the most popular vegetables,[25] *S. lycopersicum* was also chosen as the research object. *A. thaliana* seeds were soaked in 70% ethanol for 10 minutes and 5% sodium hypochlorite for 5 minutes and washed several times in sterile water. The seeds were then placed onto solid MS medium (containing 1% sucrose) and kept at 4 °C in darkness for 2 days for devernalization. Afterwards, the seeds were moved to an illumination incubator and cultivated at 21–23 °C under a 16 h light/8 h dark photoperiod for approximately 7 days. After germination, seedlings were transplanted into pots containing a mixture of vermiculite and peat soil (v/v = 1 : 2) and cultivated for 5 weeks before use. Similar procedures but without devernalization were carried out for *S. lycopersicum* cultivation.

2.4 Disk diffusion tests

Disk diffusion tests were performed according to the standard procedures published by the Clinical and Laboratory Standards Institute.[26,27] Briefly, approximately five colonies of a fungus that were at least 1 mm in diameter were collected and then suspended in sterile distilled water. The turbidity of the resulting suspension was then adjusted to 0.5 McFarland standard at a wavelength of 530 nm, and diluted tenfold with sterile distilled water to obtain the spore suspension with a concentration of 5×10^6 spores per mL. Being dipped in the spore suspension for 5 s, a cotton swab was streaked three times across the PDA or OA medium of plates. About 10 minutes later, paper disks with Au NPs, imazalil or sterile water were placed on the surface of the media, and the plates were incubated at 28 °C for 6–7 days. Finally, the plates with the inhibition zone were photographed, while the zone areas were measured using ImageJ software. Three replicates were performed for each treatment.

2.5 Observations of fungi

A PI staining experiment was conducted to explore the effect of MI-Au NPs on the integrity of the cell membrane of *B. cinerea*. First, *B. cinerea* spore suspensions with a concentration of 1×10^7 spores per mL were cultured in PDB medium mixed with MI-Au NPs (0–200 μg mL^{-1}) at 28 °C and 220 rpm for 12 h. The solutions were then centrifuged at 8000 rpm for 3 mins and washed with 10 mmol L^{-1} PBS twice. We incubated the cell suspensions with an equal volume of the PI solution (3 μM in PBS) at 28 °C in darkness for 30 minutes and washed them with PBS twice, and 20 μL of samples were placed on a glass slide with a glass coverslip. The samples were observed using a LSCM (Leica Stellaris 8, Germany) in the fluorescence and differential interference contrast (DIC) mode, with excitation at 535 nm and emissions at 605–700 nm.[19,28] The cells penetrated by MI-Au NPs were stained with PI.

The influence of MI-Au NPs on the fungal morphology and ultrastructure was examined by TEM, according to the literature.[19] After co-cultivation with 100 μg mL^{-1} MI-Au NPs for 6 days, *B. cinerea* samples from the edge of the inhibition zone were collected and fixed with 2.5% glutaraldehyde for 3–4 h, washed twice with PBS, and further fixed with 1% OsO_4 for 2 h. We then washed the samples three times with PBS, dehydrated them by successive washing with 30%, 50%, 70%, 90%, 95%, and 100% in ethanol (v/v, in water), and 50% ethanol in acetone for 10 minutes each time, and finally

dehydrated them with pure acetone twice for 10 minutes. The dehydrated samples were embedded in SPI-Pon 812 resin (Sigma-Aldrich, USA) and polymerized at 60 °C for 24 h. The embedded samples were then cut into super-thin slices, placed on Formvar-coated grids and observed by TEM at an accelerating voltage of 80 kV and using EDS (Tecnai G2 F20 U-TWIN, FEI, USA).

2.6 Fungal infection assay

Detached leaf experiments and pot experiments were performed to test the ability of MI-Au NPs to protect plants (*i.e.*, *A. thaliana* and *S. lycopersicum*) against fungal infection. Among the fungi susceptible to MI-Au NP treatment, *B. cinerea* can infect more than 200 kinds of plants and cause an annual loss of US$10–$100 billion,[29,30] thus making it the second fungal pathogen in molecular plant pathology.[2] Meanwhile, *B. cinerea* can infect the plants used in this study with obvious pathogenic characteristics (*i.e.*, leaf lesion) and high morbidity stability. The methods for its infection analysis have been established, so it is selected for the plant infection study. Data obtained from plant experiments were derived from at least ten biologically independent groups.

In the detached leaf experiment, 5-week-old plants were first sprayed with 10 mL of MI-Au NPs (100 μg mL^{-1}), imazalil (100 μg mL^{-1}) or mock solution (0.05% Tween 20). Two days later, the 7th–9th rosette leaves of *A. thaliana* were collected and placed on 0.8% agar plates. Afterwards, the leaves were inoculated with 10 μL of *B. cinerea* spore suspension (1.0×10^5 spores mL^{-1}) or PDB, cultured at 60% humidity in darkness for 3–4 days, and photographed. Lesion areas caused by *B. cinerea* were measured using ImageJ software. The experimental processes for *S. lycopersicum* were similar, except that leaves were collected from the terminal positions of the 5-week-old lateral branches.[29,31,32]

In the pot experiments, 5-week-old plants were first sprayed with 10 mL of MI-Au NPs (100 μg mL^{-1}), imazalil (100 μg mL^{-1}) or mock solution (0.05% Tween 20). Two days later, they were sprayed with 10 mL of *B. cinerea* spore suspension ($0.5–1.0 \times 10^6$ spores per mL) or PDB, and then cultivated in a growth chamber at 21–23 °C (60% humidity) with a 10 h light/14 h dark cycle for 3–5 days. Finally, the phenotypes of plants were photographed, and disease incidence was calculated as the number of infected leaves per plant divided by the total number of leaves per plant.[29,33]

2.7 Preliminary safety assessment of MI-Au NPs

Five days after the spraying of MI-Au NPs (100 μg mL^{-1}), leaves of the 5-week-old *A. thaliana* were collected, dried and fixed onto aluminum stubs using high-vacuum carbon adhesive. Next, they were coated with a platinum film[34] and examined by SEM equipped with EDS (S-4800, Hitachi, Japan). Leaves to be examined by TEM were cleaned, dried, and sectioned into approximately 1 mm^2 fragments.[35] These fragments were immersed in PBS containing 2.5% glutaraldehyde (pH = 7 and 0.1 mol L^{-1}) for 3.5 h and in 1% OsO_4 for 2 h, dehydrated by successive washing with 50%, 70%, 80%, 90%, 95%, and 100% ethanol (v/v, in water) and 100% acetone for 10 minutes each time. Then, they were embedded in epoxy resin, ultrasectioned to 60–80 nm using an ultramicrotome (Leica UC7, Germany), and strained with uranyl acetate and lead citrate for 15 minutes. The stained sections were fixed onto nickel grids for TEM analysis.[32,34,36]

S. lycopersicum seeds were washed twice with ultrapure water, disinfected in 20% sodium hypochlorite for 30 minutes, and rinsed successively with an appropriate volume of deionized Na_2-EDTA (20 mmol mL^{-1}) and ultrapure water. The seeds were then immersed in MI-Au NP solutions (0, 10, 50, 100, and 200 μg mL^{-1}) for 4 hours, and placed onto the filter papers with corresponding concentrations of MI-Au NPs. Afterwards, they were cultivated at 25 °C (80% humidity) in darkness, and the germination rate was calculated 7 days later.[37]

When having two true leaves, *S. lycopersicum* seedlings were transplanted into nursery pots. Seven days later, the seedlings were sprayed with MI-Au NPs (0–200 μg mL^{-1}), twice every day for 15 days. Subsequently, the chlorophylls and carotenoid contents of the seedlings were determined using an 80% acetone method, whereas the superoxide dismutase (SOD) activity was measured using the NBT method.[38]

Cell viability was determined using Cell Counting Kit-8 (CCK-8), according to the manufacturer's protocol (Beyotime, Shanghai, China). Specifically, cryopreserved HUVECs were activated and cultured in the cell complete medium (CCM) that is composed of 89% DMEM, 10% FBS, and 1% penicillin–streptomycin solution at 37 °C in 5% CO_2 for 24 h. Subsequently, the HUVECs were harvested, resuspended in CCM, and transferred to a 96-well plate to give a concentration of 1×10^4 cells per well. The cells were incubated at 37 °C in 5% CO_2 overnight. Afterwards, the CCM in the wells was replaced by MI-Au NPs with selected concentrations (12.5 to 200 μg mL^{-1}), and the HUVECs were further cultured statically for 24 h. Finally, the MI-Au NP solutions were removed and replaced by CCK-8 solution (10% in CCM), and the cells were incubated at 37 °C in 5% CO_2 for 2 h before microscopic observation. The morphology of HUVECs was observed using a fully automated inverted optical microscope (IX83P2ZF, Olympus, Japan). Except that the HUVECs were not treated by MI-Au NPs, operations to the control groups were the same as the experimental groups. Wells with only CCK-8 solution were used as the blank. These experiments were performed six times.[39]

2.8 Statistical analysis

The percentage of penetrated cells was determined as the mean of PI-stained spores under three microscopic vision fields of two independent experiments (each field contained 30–100 cells), as described in Eqn (1):

$$\text{Penetrated cells } (\%) = \frac{N_1}{N_2} \times 100\% \quad (1)$$

where N_1 is the number of red-fluorescent spores in every vision field and N_2 is the total number of spores in every vision field.

The viability of HUVECs was determined from the measurement of their OD450 values, as described below:

$$\text{Cell viability } (\%) = \frac{A_s - A_b}{A_c - A_b} \times 100\% \quad (2)$$

where A_s is the OD_{450} value of the experimental group, A_c is the OD_{450} value of the control group, and A_b is the OD_{450} value of the blank.

In this study, comparisons among multiple experimental groups were conducted using a one-way ANOVA with Tukey's multiple range test or Student's *t* test. Data were shown in the form of mean ± standard deviation.

3 Results and discussion

3.1 Synthesis and characterization of Au NPs

Au NPs were characterized by TEM, ICP-OES, and dynamic light scattering and zeta potential measurements. The TEM images showed that MI-Au NPs, D-Au NPs, and N-Au NPs were morphologically regular and formed uniform dispersions (Fig. 2a–c). The concentrations of MI-Au NPs, D-Au NPs, and N-Au NPs were 232.5, 770.5, and 762.3 μg mL^{-1}, respectively. Their average hydrodynamic sizes were 8.04 ± 0.06, 11.08 ± 0.08, and 6.10 ± 0.13 nm, respectively (Fig. 2d–f). The zeta potentials of MI-Au NPs, D-Au NPs, and N-Au NPs were 14.8, 17.8, and −17.6 mV, demonstrating that the surfaces of these small molecule ligand-modified Au NPs were positively charged (Fig. 2g–i).

3.2 Inhibitory effect of Au NPs on plant pathogenic fungi

The influence of MI-Au NPs, D-Au NPs, and N-Au NPs on *Magnaporthe oryzae*, *Botrytis cinerea*, *Colletotrichum destructivum*, *Fusarium oxysporum*, *Fusarium pseudograminearum*, and *Fusarium graminearum* were performed by disk diffusion tests, investigating the antifungal activity of Au NPs with different functional ligands. According to Fig. 3, all fungi grew well on the PDA plates with paper disks (containing N-Au NPs), suggesting that the fungi were not affected by the NPs. Similar to N-Au NPs, D-Au NPs did not inhibit the growth of any fungi, even at a concentration of 50 μg mL^{-1}. In contrast, the hyphal growth of *M. oryzae*, *B. cinerea*, *F. pseudograminearum* and *C. destructivum* was inhibited when MI-Au NPs was applied, even at a low concentration of 5 μg mL^{-1} (middle panel of Fig. 3 and Fig. S1, ESI†). This indicates that Au NPs capped with 2-mercaptoimidazole (MI) have stronger antifungal activity than that capped with 4,6-diamino-2-pyrimidinethiol (DAPT), which agrees with the research that groups on the surface can affect the function of Au NPs directly.[16,20] MI is reported to be a potential lead molecule for the synthesis of compounds with good antifungal activity.[40–43] Meanwhile, the smaller particle size and positive charge of MI-Au NPs can also contribute to its greater antifungal activity than the other two.[44,45]

Next, we compared the activities of MI-Au NPs and a traditional chemical fungicide (*i.e.*, imazalil) against the four selected plant pathogenic fungi. In line with the results of the previous experiment, MI-Au NPs stably inhibited the hyphal growth of the fungi at all concentrations (Fig. 4). In particular, the inhibition zones of *F. pseudograminearum* and *C. destructivum* were the largest when 100 μg mL^{-1} MI-Au NPs was used (Fig. S2, ESI†). In comparison, imazalil did not inhibit the

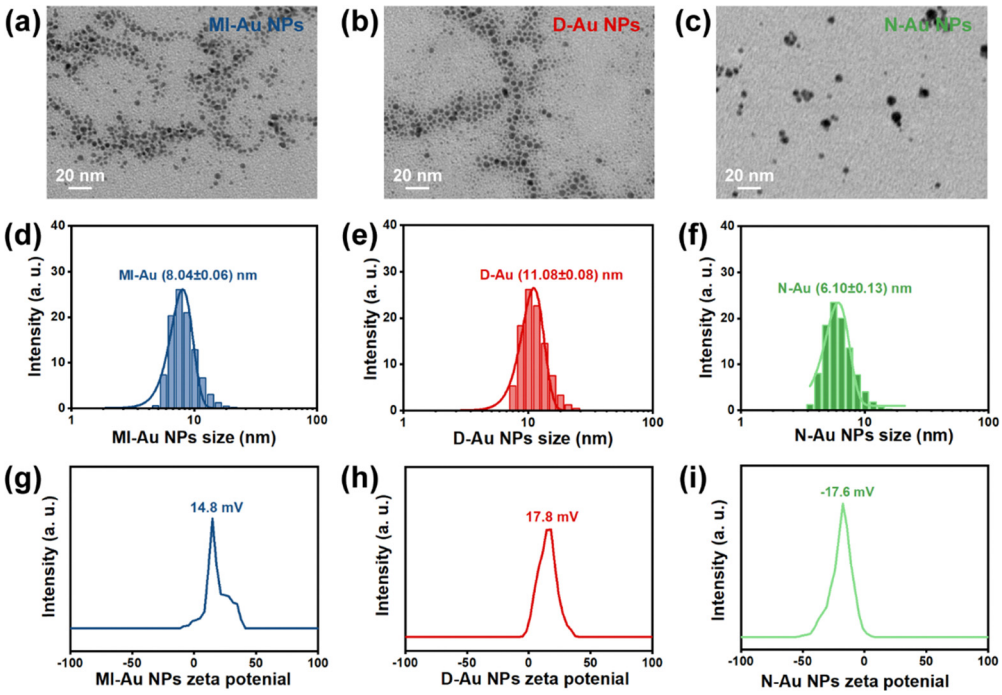

Fig. 2 The characterization of Au NPs. (a)–(c) The TEM images of Au NPs. (d)–(f) The hydrodynamic sizes of Au NPs. (g)–(i) The zeta potentials of Au NPs.

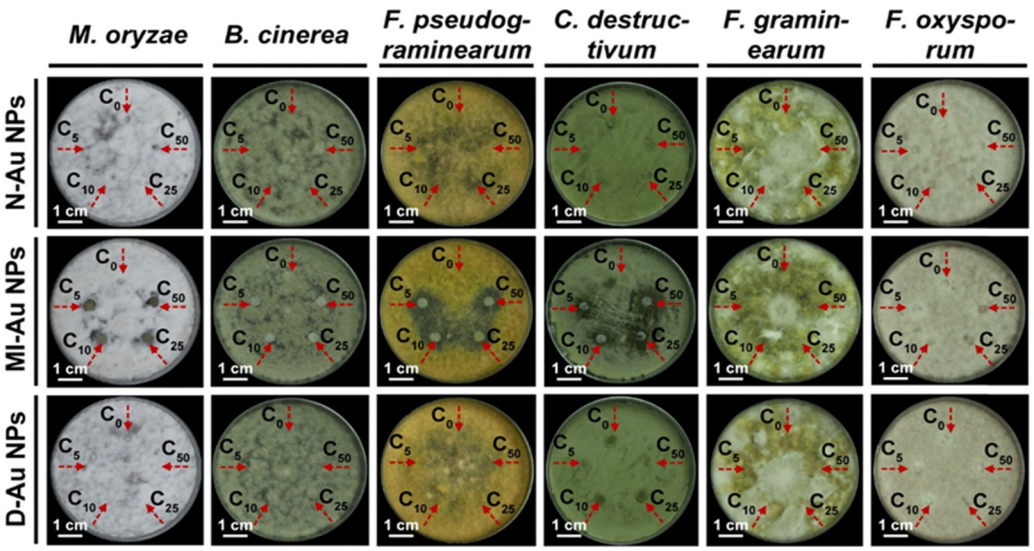

Fig. 3 Inhibitory effects of Au NPs on selected plant pathogenic fungi (C_0 = 0 μg mL^{-1}, C_5 = 5 μg mL^{-1}, C_{10} = 10 μg mL^{-1}, C_{25} = 25 μg mL^{-1}, and C_{50} = 50 μg mL^{-1}).

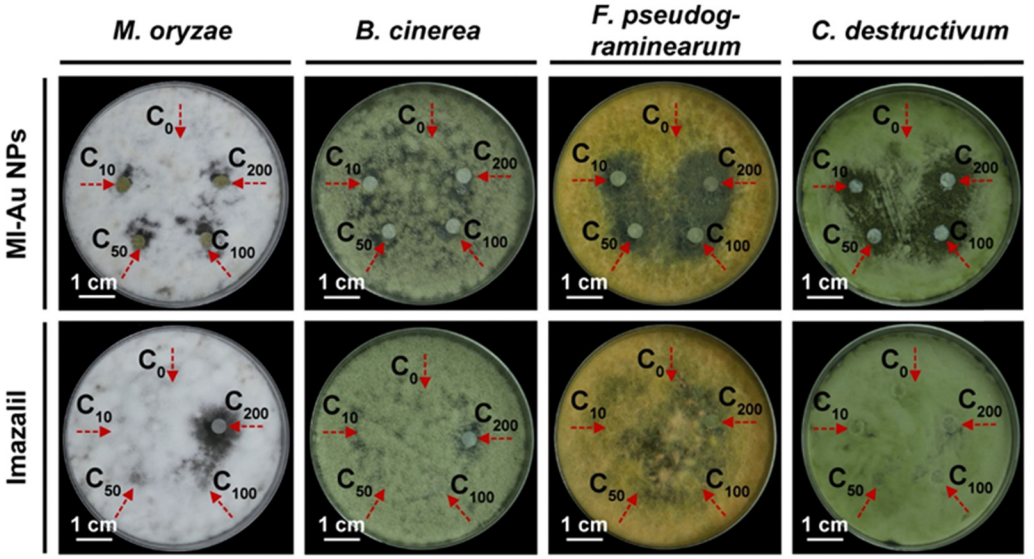

Fig. 4 Inhibitory effects of MI-Au NPs and imazalil on selected plant pathogenic fungi (C_0 = 0 μg mL^{-1}, C_{10} = 10 μg mL^{-1}, C_{50} = 50 μg mL^{-1}, C_{100} = 100 μg mL^{-1}, and C_{200} = 200 μg mL^{-1}).

growth of the fungi at the commonly used concentration of 50 μg mL^{-1}.[46] In fact, the inhibition of *M. oryzae* and *B. cinerea* by imazalil was only observed when its concentration reached 200 μg mL^{-1}, which is the highest concentration ever recommended in research.[47] Nevertheless, the application of imazail at this concentration did not impede the growth of *F. pseudograminearum* and *C. destructivum*.

3.3 Antifungal mechanisms of MI-Au NPs

In order to elucidate how the MI-Au NPs inhibited the fungi, the effect of MI-Au NPs on the integrity of *B. cinerea* was probed by staining cells with propidium iodide (PI) and then examined by LSCM.[28,48] As shown in Fig. 5a, when observed in the fluorescence mode, the amount of red stained *B. cinerea* cells (mainly spores) and their debris increased as the concentration of MI-Au NPs used increased from 10 μg mL^{-1} to 200 μg mL^{-1}, whereas there was almost no red color observed in the group without MI-Au NPs. Pictures in the merge mode (overlay of fluorescence and DIC images) supported this observation. As PI can stain nucleic acids but cannot penetrate the membrane of viable cells,[28] the above-described results indicated that the red-colored cells were not intact, confirming that MI-Au NPs disrupted the cell membrane of *B. cinerea*. Importantly, with an increase in the concentration of NPs from 10 μg mL^{-1} to

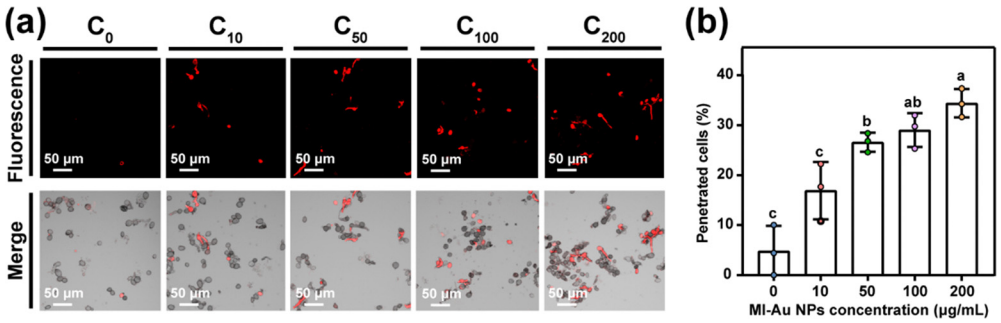

Fig. 5 MI-Au NPs' penetration of the cell membrane. (a) Images of the *B. cinerea* cells (mainly spores) stained by PI in the fluorescence mode (upper panel) and merge mode (lower panel). (b) Percentage of spores with the membrane penetrated by MI-Au NPs (C_0 = 0 μg mL^{-1}, C_{10} = 10 μg mL^{-1}, C_{50} = 50 μg mL^{-1}, C_{100} = 100 μg mL^{-1}, and C_{200} = 200 μg mL^{-1}). Different lower-case letters denote statistically significant differences ($p < 0.05$) between bars. Error bars indicate the standard deviation of the mean.

200 μg mL^{-1}, the proportion of penetrated spores increased from 16.9% to 34.4% ($p < 0.001$) (Fig. 5b). This suggests that MI-Au NPs alter the membrane integrity in a dose-dependent manner.

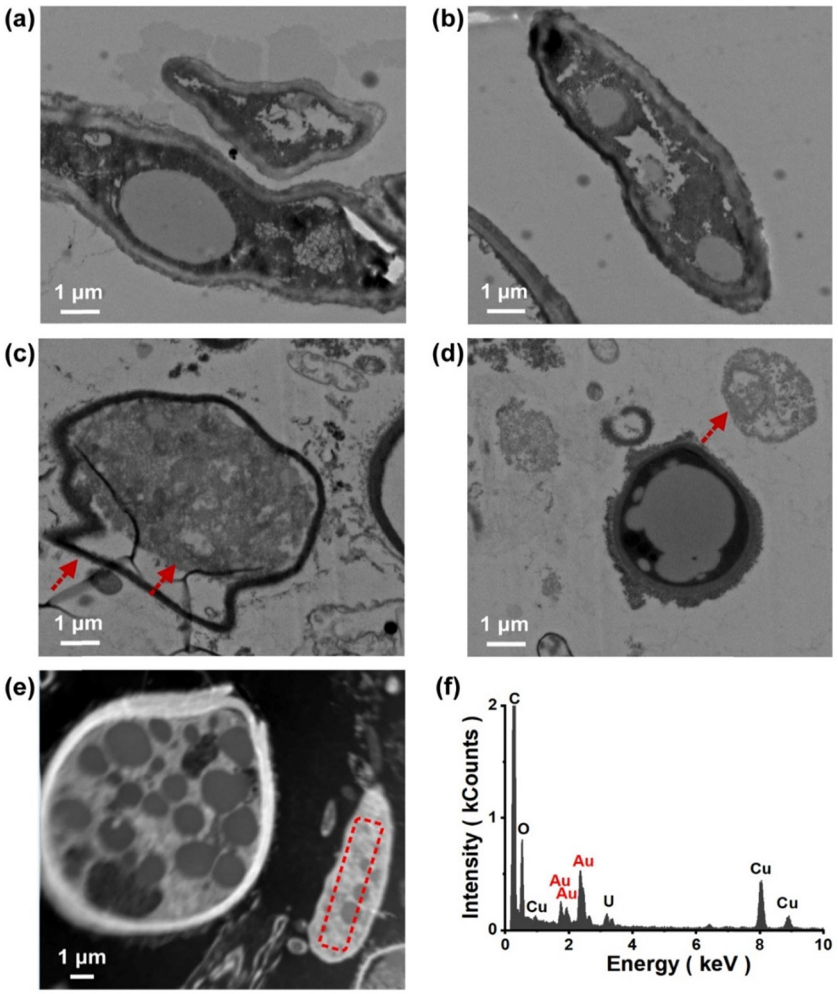

Fig. 6 TEM pictures of *B. cinerea* upon treatment with MI-Au NPs. (a) and (b) Typical ultrastructure of *B. cinerea* hyphae without MI-Au NP treatment. (c) Ruptured plasma membrane detached from the spore wall (red arrows) after having been treated with MI-Au NPs. (d) Left-over of the disrupted spore (red arrows). (e) *B. cinerea* spore treated with 100 μg mL^{-1} MI-Au NPs. (f) Energy-dispersive analysis spectrum of the region outlined by the red dashed lines in (e).

Next, TEM was used to directly visualize the change in the morphology of the *B. cinerea* membrane and the leakage of nucleic acids upon treatment with MI-Au NPs. Untreated cells had normal morphologies with an orderly and intact plasma membrane (Fig. 6a and b). However, cells treated with 100 μg mL^{-1} MI-Au NPs had been destroyed, and some spores had abnormal morphologies (Fig. 6c), which resulted in cytoplasmic leakage (Fig. 6d). This is consistent with the results of the PI staining experiment. Moreover, the mixtures of the leaked cytoplasm and MI-Au NPs appeared as a clustered dot structure, indicating that MI-Au NPs may have interacted with nucleic acids.[19,49] The distribution of Au within the spores of *B. cinerea* was confirmed by energy dispersive spectrometry (EDS) (Fig. 6e and f), indicating that MI-Au NPs can pass through the cell wall and membrane of *B. cinerea*. The damage to *B. cinerea* caused by MI-Au NPs is similar to that caused by cationic antibiotics such as polymyxin and gentamicin,[50,51] suggesting that MI-Au NPs may have a broad-spectrum antifungal activity.

3.4 Application of MI-Au NPs as antifungal agents in plants

3.4.1 Antifungal activity of MI-Au NPs on detached leaves. Given that MI-Au NPs performed better than imazalil in the inhibition of the selected plant pathogenic fungi in the disk diffusion test, their potential to protect plants from *B. cinerea* infection was investigated.

Detached leaves that were pretreated with mock solution, MI-Au NPs and imazalil, but not inoculated with *B. cinerea* spores were green and healthy (left panel of Fig. 7a), showing that the leaves were not negatively affected by these pretreatments. In comparison, leaves inoculated with *B. cinerea* spores

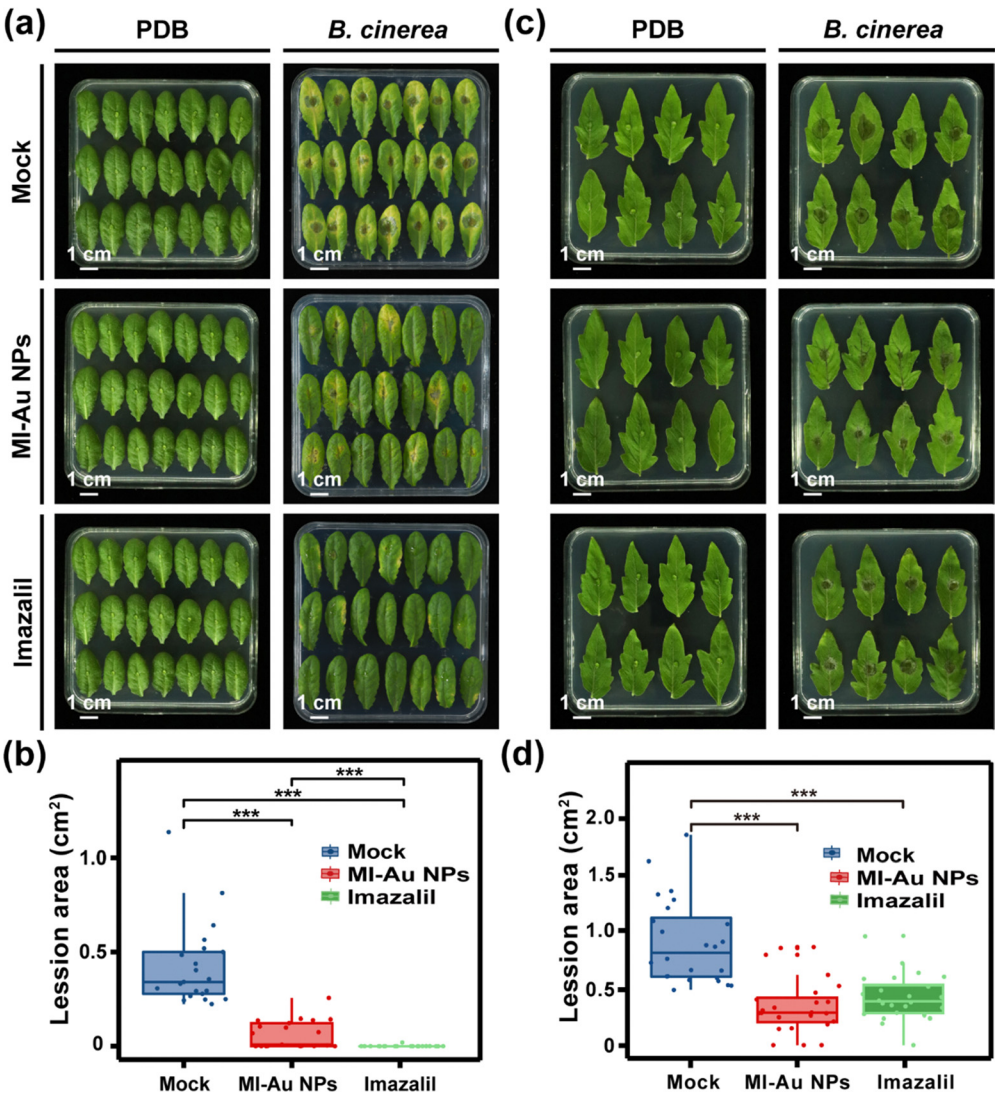

Fig. 7 Infection of *A. thaliana* leaves and *S. lycopersicum* leaves with *B. cinerea*. (a) Phenotypes of detached *A. thaliana* leaves 4 days after inoculation with *B. cinerea* spores (right panel) or PDB (medium for *B. cinerea*, left panel). (b) Average lesion area on detached *A. thaliana* leaves infected with *B. cinerea* (n = 21). (c) Phenotypes of detached *S. lycopersicum* leaves 3 days after inoculation with *B. cinerea* spores (right panel) or PDB (left panel). (d) Average area of lesions on detached *S. lycopersicum* leaves infected with *B. cinerea* (n = 24). Asterisks denote statistically significant differences (**: $p < 0.01$; ***: $p < 0.001$).

turned yellow (right panel of Fig. 7a) and had rather large lesions. A 100% incidence rate of *B. cinerea* to the leaves was observed, demonstrating the strong pathogenicity of *B. cinerea* to *A. thaliana*. However, leaves that had been pretreated with MI-Au NPs prior to inoculation with *B. cinerea* spores remained generally green, and the incidence rate was approximately 70% less than that of the mock group. Similarly, the average lesion area on the MI-Au NP-pretreated leaves (0.062 cm^2) was 85.4% less than that on the mock-solution-pretreated leaves (0.425 cm^2, Fig. 7b; $p < 0.001$), demonstrating that MI-Au NPs could protect *A. thaliana* from *B. cinerea* infection. Imazalil could also protect leaves from *B. cinerea* infection, and the average lesion area of imazalil-pretreated leaves was 99.3% less than that of mock-solution-pretreated leaves (Fig. 7b).

Consistent with the *A. thaliana* experiment results, the treatment of the agents did not have any negative effects on the leaves of *S. lycopersicum* (left panel of Fig. 7c). Moreover, among the leaves being infected with *B. cinerea*, the average lesion area on the mock solution-pretreated leaves was much larger than that on *A. thaliana* leaves (Fig. 7b and d). Furthermore, lesions appeared on all leaves 3 days after inoculation with *B. cinerea*, irrespective of whether the leaves had been pretreated with the antifungal agents (right panel of Fig. 7c), indicating that *B. cinerea* was more pathogenic to *S. lycopersicum* than to *A. thaliana*. Nevertheless, the average lesion areas on the MI-Au NP- and imazalil-pretreated leaves were much smaller than the mock-solution-pretreated leaves (both $p < 0.001$, Fig. 7d).

3.4.2 Antifungal activity of MI-Au NPs on live plants. Given that MI-Au NPs exhibited good antifungal effects in detached leaves experiments, their activity on live plants was examined in pot experiments. As shown in the right panel of Fig. 8a, more than half of the *A. thaliana* leaves inoculated with *B. cinerea* (pretreated by mock solution) turned yellow, and the average disease incidence rate arrived at approximately 74.6% (Fig. 8b). In comparison, the average disease incidence rate in the plants pretreated with MI-Au NPs was 91.7% less than that in the mock group (6.2% *vs.* 74.6%; Fig. 8b). Imazalil pretreatment also decreased the disease incidence rate (to 23.8%, $p < 0.001$,

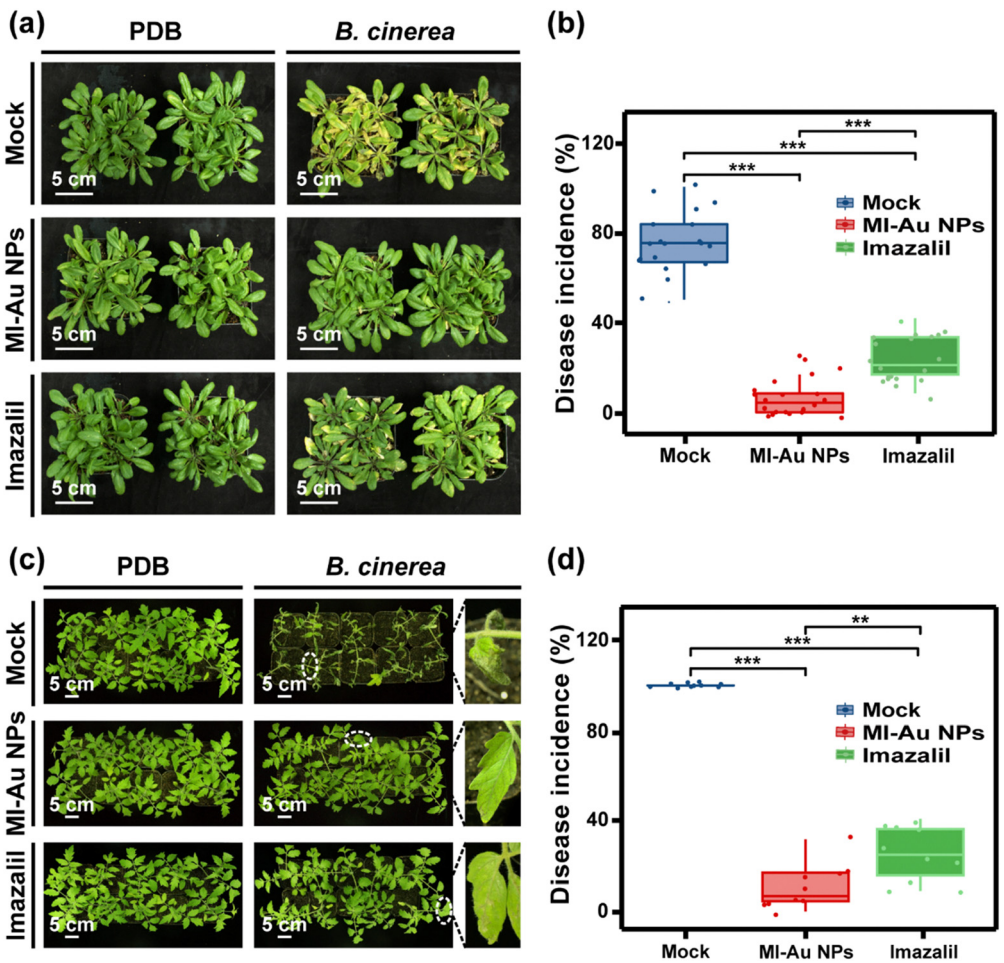

Fig. 8 Infection of *A. thaliana* and *S. lycopersicum* with *B. cinerea*. (a) Phenotypes of *A. thaliana* 5 days after inoculation with *B. cinerea* spores (right panel) or PDB (left panel). (b) Average disease incidence rate of *A. thaliana* infected with *B. cinerea* (n = 20 individual plants). (c) Phenotypes of *S. lycopersicum* 4 days after inoculation with *B. cinerea* spores (right panel) or PDB (left panel), and a magnified view of the area enclosed with the dashed ellipses. (d) Average disease incidence rate of *S. lycopersicum* infected with *B. cinerea* (n = 10 individual plants). Asterisks denote statistically significant differences (**: $p < 0.01$; ***: $p < 0.001$).

Fig. 8b), but the effect was less obvious than that obtained by MI-Au NPs.

With regard to *S. lycopersicum* (left panel of Fig. 8c), B. *cinerea* infection caused more serious disease than that in *A. thaliana* (Fig. 8a and c). Most of the *S. lycopersicum* leaves were wilted with large grey lesions on them, and the disease incidence rate was almost 100% (Fig. 8b and d). This is consistent with the detached leaf experiment results and confirms the strong pathogenicity of *B. cinerea* towards *S. lycopersicum* plants. Pretreatment of *S. lycopersicum* plants with imazalil reduced necrosis of the leaves caused by *B. cinerea* infection, and the disease incidence of 25.5% further indicated the effective protection of imazalil for *S. lycopersicum* plants. More importantly, the pretreatment of *S. lycopersicum* plants with MI-Au NPs significantly reduced the necrosis of leaves caused by *B. cinerea* infection. The leaves remained lush and green, and the disease incidence rate was only 10.9% ($p < 0.001$), which was 10.9% and 42.7% of that in the mock- and imazalil-pretreated plants, respectively (Fig. 8d).

In general, MI-Au NPs were demonstrated to be effective in protecting plants from *B. cinerea* infection. The protection effect was especially obvious on *S. lycopersicum*, even compared

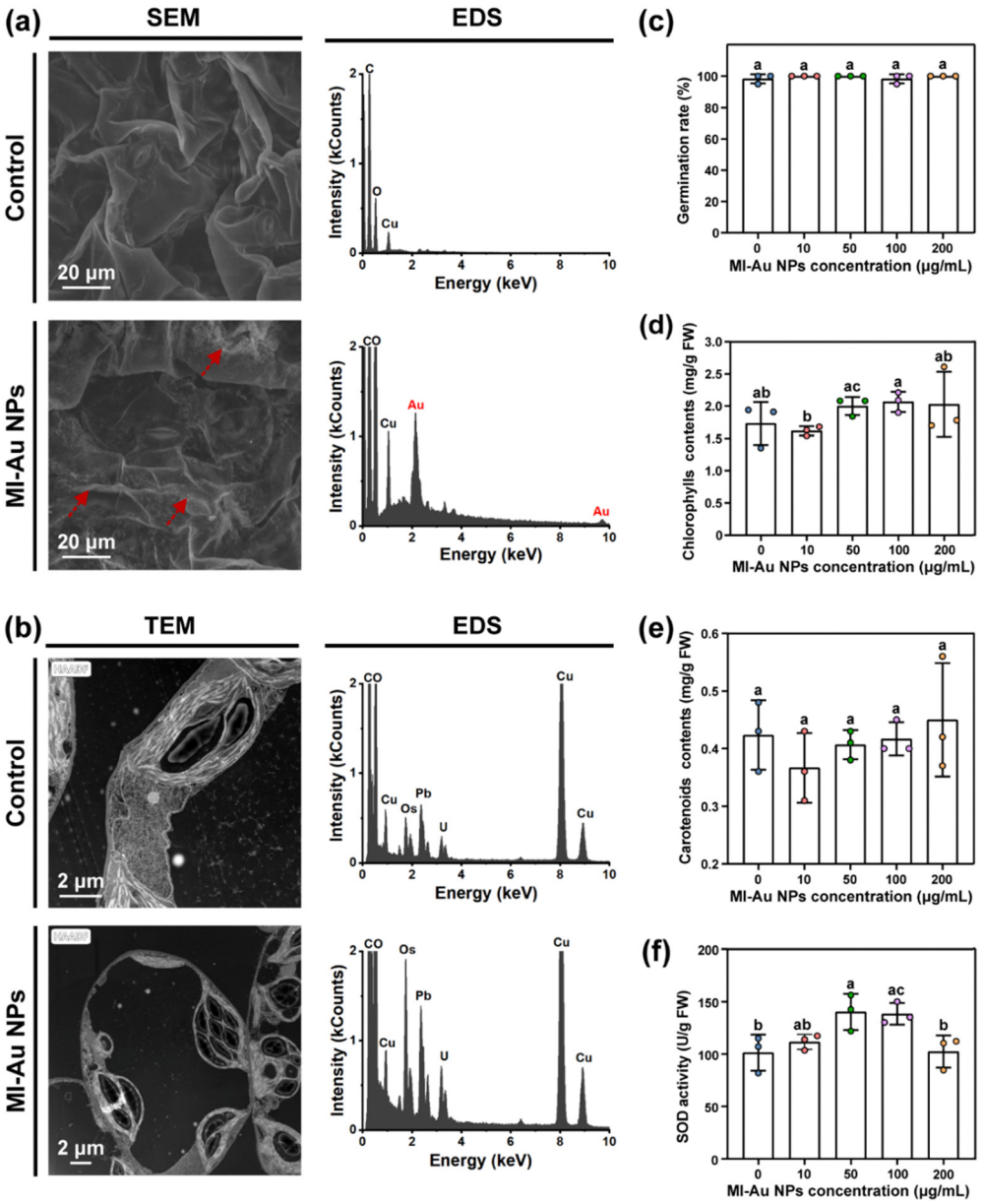

Fig. 9 Biotoxicity of MI-Au NPs to plants. (a) SEM and corresponding EDS images of the leaf surface not exposed to MI-Au NPs (upper panel) or exposed to MI-Au NPs (lower panel). (b) TEM and corresponding EDS images of the super thin leaf sample not exposed to MI-Au NPs (upper panel) or exposed to MI-Au NPs (lower panel). (c) Influence of MI-Au NPs on the germination of *S. lycopersicum* seeds. (d) Contents of chlorophylls. (e) Contents of carotenoids. (f) SOD activity. Different lowercase letters denote statistically significant differences ($p < 0.05$) between bars. Error bars indicate the standard deviation of the mean.

with the results achieved by imazalil. This may owe to the differences between the leaf surfaces of the two plants: the trichomes on the surface of *S. lycopersicum* leaves are denser and longer than that of *A. thaliana* leaves.[52–54] Therefore, *S. lycopersicum* leaves are more hydrophobic than *A. thaliana* leaves, which could impede the effective contact of imazalil solution to *S. lycopersicum* leaves and reduce the residence time on them. However, NPs could effectively come into contact with the hydrophobic leaf surfaces.[55]

3.5 Biotoxicity of MI-Au NPs

The biocompatibility of Au NPs should be confirmed to support their application in agriculture. Thus, we explored whether MI-Au NPs affected the growth or development of plants and HUVECs, respectively.

3.5.1 Phytotoxicity assay. As shown in the upper panel of Fig. 9a, the surface of the leaf that was not pretreated with MI-Au NPs was free of particles. In contrast, the leaf pretreated with MI-Au NPs bore a dispersion of fine particles (lower panel of Fig. 9a), as seen by SEM. This was confirmed by the corresponding EDS that contained a rather intense peak for Au (lower panel of Fig. 9a). Subsequently, the super-thin slices of leaf samples were taken and analyzed to investigate whether the MI-Au NPs penetrated the cuticular layer and entered the cells. The TEM and corresponding EDS images of the super-thin slices revealed that there was no Au in cuticular layers or intracellular areas of samples, irrespective of whether they had been treated with MI-Au NPs (Fig. 9b). This suggests that owing to the relatively large hydration radii of the MI-Au NPs (8.04 ± 0.06 nm), they cannot pass through the holes (diameter < 5 nm) in the cuticles of leaves.[56]

As one of the indicators to evaluate the phytotoxicity of chemical substances,[35,37,57] the influence of MI-Au NPs on plant germination was evaluated. The results showed that the

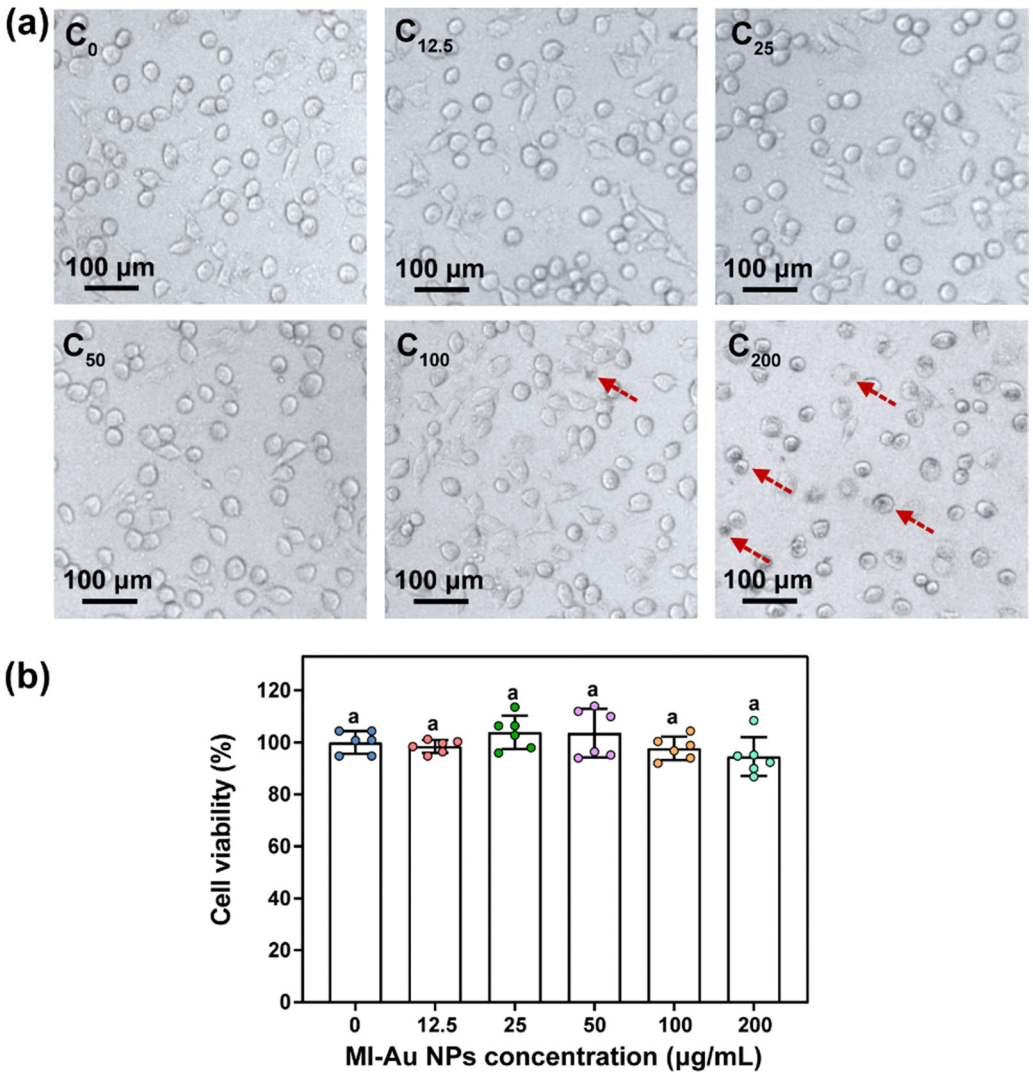

Fig. 10 Cytotoxicity of MI-Au NPs to HUVECs. (a) Morphologies of HUVECs treated with MI-Au NPs (red dashed arrows indicate cells with NP aggregation). (b) Statistical analysis of the viability of HUVECs treated with various concentrations of MI-Au NPs ($n = 6$). Different lowercase letters denote statistically significant differences ($p < 0.05$) between bars. Error bars indicate the standard deviation of the mean.

germination of *S. lycopersicum* seeds was not inhibited by MI-Au NPs: all seeds germinated within 7 days, regardless of the concentration of MI-Au NPs applied (Fig. 9c and Fig. S3, ESI†). In contrast, NPs were previously reported to increase the germination and growth of wheat.[58]

As indicators to evaluate the plant's response to biotic and abiotic stresses, the effect of MI-Au NP treatment on the accumulation of chlorophylls and carotenoids, and the superoxide dismutase (SOD) activity of plants was measured.[37] As shown in Fig. 9d and e, MI-Au NP-treatment caused changes in the content of chlorophylls from 1.5 mg g^{-1} to 2.0 mg g^{-1}, whereas the contents of carotenoids stabilized at approximately 0.4 mg g^{-1}. However, the contents were not significantly different from those observed in the control groups. As shown in Fig. 9f, plants treated with 50–100 μg mL^{-1} MI-Au NPs exhibited a 38.4% increase in SOD activity.

3.5.2 Cytotoxicity assay on HUVECs. The effect of MI-Au NPs on HUVECs was tested using Cell Counting Kit-8. As shown in Fig. 10a, the HUVECs treated with MI-Au NPs at concentrations ranging from 12.5 μg mL^{-1} to 100 μg mL^{-1} appeared to be spherical and flat in shape, which was similar to that of HUVECs in the untreated control group (0 μg mL^{-1}), indicating that the cell morphology remained normal in the presence of MI-Au NPs. Some HUVECs exposed to 200 μg mL^{-1} MI-Au NPs became dark due to the aggregation of MI-Au NPs on HUVECs, and a small proportion of HUVEC membranes ruptured. However, no statistically significant difference in HUVEC viability was observed as the concentration of MI-Au NPs increased from 12.5 μg mL^{-1} to 200 μg mL^{-1} (Fig. 10b). This indicates that MI-Au NPs can be regarded as non-cytotoxic to mammalian cells, especially when considering that the highest working concentration of MI-Au NPs was normally 100 μg mL^{-1}.

4 Conclusions

This study presents the first evidence that Au NPs could be a viable alternative for the management of plant pathogenic fungi, as they could specifically inhibit the activity of fungi by destroying their morphology without damage to the plants. MI-Au NPs exhibited a strong inhibitory effect against the selected 'top' plant pathogenic fungi and effectively prevented the infection of *B. cinerea* to the plants of *A. thaliana* and *S. lycopersicum*. The good biocompatibility of MI-Au NPs further demonstrated their safety for use as antifungal agents in labs. In general, this study has important implications for the development of nanoparticle-based antifungal agents to solve the drug-resistant problem of fungi and may promote green and high-quality agricultural development.

Author contributions

Tang Xu and Wenshuai Hao: conceptualization, validation, writing – original draft, writing – review & editing, and formal analysis. Ran Du: methodology, visualization, and writing – review & editing. Dai Dai, Cuixia Wang and Carol Sze Ki Lin: writing – review & editing, and validation. Suhua Li: methodology, investigation, and validation. Chong Li, Jianbin Yan and Ruitao Cha: conceptualization, data curation, writing – review & editing, formal analysis, project administration, resources, and supervision.

Data availability

The data that support the findings of this study are available from the corresponding author (C. Li) upon reasonable request.

Conflicts of interest

There are no conflicts to declare.

Acknowledgements

The authors acknowledge funds from the National Key R&D Program of China (2023ZD04076), the Science and Technology Innovation Project of Foshan (2320001006040), and the Scientific Research Foundation for Principal Investigator (KIMA-QD2022005) of Kunpeng Institute of Modern Agriculture at Foshan, Chinese Academy of Agricultural Sciences. Many thanks to Prof. Qun Liu of the China National Rice Research Institute and Dr Chengqi Zhang from Anhui Agricultural University for providing fungi used in this study.

References

1 U.S. Department of Agriculture, **https://www.ars.usda.gov/oc/dof/food-security-how-do-crop-plants-combat-pathogens/**, (accessed 25 April 2024).
2 R. Dean, J. a L. Van Kan, Z. A. Pretorius, K. E. Hammond-Kosack, A. Di Pietro, P. D. Spanu, J. J. Rudd, M. Dickman, R. Kahmann, J. Ellis and G. D. Foster, *Mol. Plant Pathol.*, 2012, **13**, 414–430.
3 L. Boddy, Pathogens of Autotrophs, in *The Fungi*, ed. S. C. Watkinson, L. Boddy and N. P. Money, Academic Press, Boston, 2016, pp. 245–292.
4 M. L. Gullino, F. Tinivella, A. Garibaldi, G. M. Kemmitt, L. Bacci and B. Sheppard, *Plant Dis.*, 2010, **94**, 1076–1087.
5 S. K. Chen, C. A. Edwards and S. Subler, *Soil Biol. Biochem.*, 2001, **33**, 1971–1980.
6 D. W. Hollomon, *Plant Prot. Sci.*, 2015, **51**, 170–176.
7 M. Hahn, *J. Chem. Biol.*, 2014, **7**, 133–141.
8 H. J. Rosslenbroich and D. Stuebler, *Crop Prot.*, 2000, **19**, 557–561.
9 L. Wang, C. Hu and L. Shao, *Int. J. Nanomed.*, 2017, **12**, 1227–1249.
10 A. J. Huh and Y. J. Kwon, *J. Controlled Release*, 2011, **156**, 128–145.
11 T. Bruna, F. Maldonado-Bravo, P. Jara and N. Caro, *Int. J. Mol. Sci.*, 2021, **22**, 7202.
12 S. W. Kim, J. H. Jung, K. Lamsal, Y. S. Kim, J. S. Min and Y. S. Lee, *Mycobiology*, 2012, **40**, 53–58.

13 I. Akpinar, M. Unal and T. Sar, *SN Appl. Sci.*, 2021, **3**, 506.
14 A. Panáček, L. Kvítek, M. Smékalová, R. Večeřová, M. Kolář, M. Röderová, F. Dyčka, M. Šebela, R. Prucek, O. Tomanec and R. Zbořil, *Nat. Nanotechnol.*, 2018, **13**, 65–71.
15 X. Gu, Z. Xu, L. Gu, H. Xu, F. Han, B. Chen and X. Pan, *Environ. Chem. Lett.*, 2021, **19**, 167–187.
16 W. Zheng, Y. Jia, Y. Zhao, J. Zhang, Y. Xie, L. Wang, X. Zhao, X. Liu, R. Tang, W. Chen and X. Jiang, *Nano Lett.*, 2021, **21**, 1992–2000.
17 C. Tao, *Lett. Appl. Microbiol.*, 2018, **67**, 537–543.
18 Y. Feng, W. Chen, Y. Jia, Y. Tian, Y. Zhao, F. Long, Y. Rui and X. Jiang, *Nanoscale*, 2016, **8**, 13223–13227.
19 Y. Zhao, Y. Tian, Y. Cui, W. Liu, W. Ma and X. Jiang, *J. Am. Chem. Soc.*, 2010, **132**, 12349–12356.
20 X. Li, S. M. Robinson, A. Gupta, K. Saha, Z. Jiang, D. F. Moyano, A. Sahar, M. A. Riley and V. M. Rotello, *ACS Nano*, 2014, **8**, 10682–10686.
21 R. Krishnamoorthi, S. Bharathakumar, B. Malaikozhundan and P. U. Mahalingam, *Biocatal. Agric. Biotechnol.*, 2021, **35**, 102107.
22 A. Almansob, A. H. Bahkali and F. Ameen, *Nanomaterials*, 2022, **12**, 814.
23 R. Kalaivani, M. Maruthupandy, T. Muneeswaran, M. Singh, S. Sureshkumar, M. Anand, C. M. Ramakritinan, F. Quero and A. K. Kumaraguru, *Int. J. Biol. Macromol.*, 2020, **146**, 560–568.
24 R. A. D. Arancon, S. H. T. Lin, G. Chen, C. S. K. Lin, J. Lai, G. Xu and R. Luque, *RSC Adv.*, 2014, **4**, 17114–17119.
25 J. Zhang, S. Liu, X. Zhu, Y. Chang, C. Wang, N. Ma, J. Wang, X. Zhang, J. Lyu and J. Xie, *Plants*, 2023, **12**, 2947.
26 R. M. Humphries, J. Ambler, S. L. Mitchell, M. Castanheira, T. Dingle, J. A. Hindler, L. Koeth and K. Sei, *J. Clin. Microbiol.*, 2018, **56**, e01934-17.
27 E. L. Berkow, S. R. Lockhart and L. Ostrosky-Zeichner, *Clin. Microbiol. Rev.*, 2020, **33**, e00069-19.
28 W. Yuan, P. Tian, A. Lyu, Y. Lyu, W. Zhang, S. Wei and Y. Hu, *Grain Oil Sci. Technol.*, 2020, **3**, 1–8.
29 Y. Li, S. Li, R. Du, J. Wang, H. Li, D. Xie and J. Yan, *Front. Plant Sci.*, 2021, **12**, 628328.
30 S. AbuQamar, K. Moustafa and L. S. Tran, *Crit. Rev. Biotechnol.*, 2017, **37**, 262–274.
31 S. Song, H. Huang, H. Gao, J. Wang, D. Wu, X. Liu, S. Yang, Q. Zhai, C. Li, T. Qi and D. Xie, *Plant Cell*, 2014, **26**, 263–279.
32 M. El-Shetehy, A. Moradi, M. Maceroni, D. Reinhardt, A. Petri-Fink, B. Rothen-Rutishauser, F. Mauch and F. Schwab, *Nat. Nanotechnol.*, 2021, **16**, 344–353.
33 X. Cao, C. Wang, X. Luo, L. Yue, J. C. White, W. Elmer, O. P. Dhankher, Z. Wang and B. Xing, *ACS Nano*, 2021, **15**, 11817–11827.
34 J. He, L. Zhang, S. Y. He, E. T. Ryser, H. Li and W. Zhang, *Environ. Pollut.*, 2022, **292**, 118448.
35 X. Wang, X. Liu, X. Yang, L. Wang, J. Yang, X. Yan, T. Liang, H. Chr Bruun Hansen, B. Yousaf, S. M. Shaheen, N. Bolan and J. Rinklebe, *Ecotoxicol. Environ. Saf.*, 2022, **242**, 113939.
36 M. Hassanisaadi, A. H. S. Bonjar, A. Rahdar, R. S. Varma, N. Ajalli and S. Pandey, *Mater. Today Commun.*, 2022, **33**, 104183.
37 X. Zhao, W. Zhang, Y. He, L. Wang, W. Li, L. Yang and G. Xing, *Chemosphere*, 2021, **263**, 127943.
38 J. F. Gao, *Experimental Guidance for Plant Physiology*, Higher Education Press, Beijing, China, 2006.
39 K. Cheng and M. Hao, *Int. J. Mol. Sci.*, 2016, **17**, 2000.
40 N. Rani and R. Dahiya, *Curr. Comput.-Aided Drug Des.*, 2017, **13**, 48–56(9).
41 N. Rani and R. Singh, *Curr. Comput.-Aided Drug Des.*, 2019, **15**, 409–420.
42 N. Rani, P. Kumar and R. Singh, *Comb. Chem. High Throughput Screening*, 2019, **22**, 89–96.
43 N. Rani and R. Singh, *Lett. Drug Des. Discovery*, 2019, **16**, 512–521.
44 P. Rajiv, S. Rajeshwari and R. Venckatesh, *Spectrochim. Acta, Part A*, 2013, **112**, 384–387.
45 A. R. Cruz-Luna, H. Cruz-Martínez, A. Vásquez-López and D. I. Medina, *J. Fungi*, 2021, **7**, 1033.
46 H. Dong, Y. He, C. Fan, Z. Zhu, C. Zhang, X. Liu, K. Qian and T. Tang, *Nanomaterials*, 2022, **12**, 3879.
47 R. Villalta, M. Sample, D. Shields and M. Guzmán Quesada, *Fitopatología*, 2006, **32**, 17–33.
48 L. Xu, N. Tao, W. Yang and G. Jing, *Ind. Crops Prod.*, 2018, **112**, 427–433.
49 L. Wang, W. Hu, J. Deng, X. Liu, J. Zhou and X. Li, *RSC Adv.*, 2019, **9**, 28987–28995.
50 M. Vaara and T. Vaara, *Antimicrob. Agents Chemother.*, 1983, **24**, 114–122.
51 J. L. Kadurugamuwa, A. J. Clarke and T. J. Beveridge, *J. Bacteriol.*, 1993, **175**, 5798–5805.
52 E. Vendemiatti, A. Zsögön, G. F. F. E. Silva, F. A. de Jesus, L. Cutri, C. R. F. Figueiredo, F. A. O. Tanaka, F. T. S. Nogueira and L. E. P. Peres, *Plant Sci.*, 2017, **259**, 35–47.
53 J.-H. Kang, F. Shi, A. D. Jones, M. D. Marks and G. A. Howe, *J. Exp. Bot.*, 2010, **61**, 1053–1064.
54 M. D. Marks, E. Gilding and J. P. Wenger, *Plant J.*, 2007, **52**, 352–361.
55 A. Avellan, J. Yun, B. P. Morais, E. T. Clement, S. M. Rodrigues and G. V. Lowry, *Environ. Sci. Technol.*, 2021, **55**, 13417–13431.
56 F. Schwab, G. Zhai, M. Kern, A. Turner, J. L. Schnoor and M. R. Wiesner, *Nanotoxicology*, 2016, **10**, 257–278.
57 D. Duan, J. Tong, Q. Xu, L. Dai, J. Ye, H. Wu, C. Xu and J. Shi, *Environ. Pollut.*, 2020, **267**, 115546.
58 A. Joshi, H. Nayyar, K. Dharamvir and G. Verma, *AIP Conf. Proc.*, 2018, **1953**, 030058.